Computers and Geosciences 109 (2017) 67–74

Contents lists available at ScienceDirect

Computers and Geosciences

journal homepage: www.elsevier.com/locate/cageo

Research paper

Classification of radiolarian images with hand-crafted and deep features

Ali Seydi Keçeli [a,*,1], Aydõn Kaya [a,1], Seda Uzunçimen Keçeli [b,1]

[a] Hacettepe University, Computer Engineering Department, 06800, Ankara, Turkey
[b] Hacettepe University, Geological Engineering Department, 06800, Ankara, Turkey

ARTICLE INFO

Keywords:
Deep learning
Image features
Radiolarian image
Pattern classification

ABSTRACT

Radiolarians are planktonic protozoa and are important biostratigraphic and paleoenvironmental indicators for paleogeographic reconstructions. Radiolarian paleontology still remains as a low cost and the one of the most convenient way to obtain dating of deep ocean sediments. Traditional methods for identifying radiolarians are time-consuming and cannot scale to the granularity or scope necessary for large-scale studies. Automated image classification will allow making these analyses promptly. In this study, a method for automatic radiolarian image classification is proposed on Scanning Electron Microscope (SEM) images of radiolarians to ease species identification of fossilized radiolarians. The proposed method uses both hand-crafted features like invariant moments, wavelet moments, Gabor features, basic morphological features and deep features obtained from a pre-trained Convolutional Neural Network (CNN). Feature selection is applied over deep features to reduce high dimensionality. Classification outcomes are analyzed to compare hand-crafted features, deep features, and their combinations. Results show that the deep features obtained from a pre-trained CNN are more discriminative comparing to hand-crafted ones. Additionally, feature selection utilizes to the computational cost of classification algorithms and have no negative effect on classification accuracy.

1. Introduction

Radiolarians are planktonic protozoa widely distributed in the oceans, throughout the water column adapted for a drifting existence. The skeleton of radiolarians is made up of pure amorphous silica and is the most characteristic morphological feature of the organism. The intricacy and the architectural diversity of the skeletons have long given rise to amazement (De Wever et al., 2002). They are important biostratigraphic and paleoenvironmental indicators for paleogeographic reconstructions. Radiolarians sensitivity makes them useful in the biostratigraphical correlation of oceanic sediments. Radiolarians have an increasing value as depth, paleoclimate, and paleotemperature indicators (Casey et al., 1990). Radiolarian paleontology still remains the cheapest and comparatively rapid way to obtain dating of deep ocean sediments (O'Dogherty et al., 2009a).

Studying fossilized radiolarians became possible after the etching technique was established and described by Dumitrica (1978) and Pessagno Jr and Newport (1972) and validated by the radiolarian paleontologists (De Wever et al., 2002). Processing patterns change with different types, but there are classical preparation procedures. The radiolarian skeletons are extracted from broken rock samples by treating them with a mixture of concentrated acids (10%) (hydrofluoric, hydrochloric, nitric, and acetic) and water (90%). After a lapsed reaction time of 24 h, washing and sieving should be performed with 63 μm and 280 μm meshes and the residue on the 63 μm must be collected. Finally, radiolarian skeletons are collected from the residue with the help of a slender brush under a binocular microscope. Those picked out are examined under Scanning Electron Microscope (SEM) for detailed taxonomic studies and illustration (De Wever et al., 2002). To identify the radiolarian to the corresponding genera and species one would need to exhaust former studies up until today. Not only morphological characters of the skeleton but also geometry and property of the shells including, the number of segments, horns, arms, feet, spicules and pores on the surface of the skeleton and the apertures are important to identify genera and species of the radiolarians. Subsequent to taxonomic studies paleontologists work on the radiolarian fauna they get and decide which time interval the sample fits in geological time scale, then paleontologist can model the biostratigraphy of the study area and can make paleogeographic interpretations. Although species classification method described above is an old-fashioned approach, it is still the only method that is used in this process. In the literature, there is not a newer approach for taxonomic classification.

* Corresponding author.
E-mail addresses: aliseydi@cs.hacettepe.edu.tr, aliseydikeceli@gmail.com (A.S. Keçeli), aydinkaya@cs.hacettepe.edu.tr (A. Kaya), sedaujeo@hacettepe.edu.tr (S.U. Keçeli).
[1] All authors have equal contribution.

http://dx.doi.org/10.1016/j.cageo.2017.08.011
Received 23 February 2017; Received in revised form 2 August 2017; Accepted 10 August 2017
Available online 16 August 2017
0098-3004/

The automatic classification problem has been explained in taxonomy studies previously. Apostol et al. (2016) proposed a method for classification of Radiolarian fossil images. A translation, rotation and scale invariant method that utilizes Fourier transform is proposed by Fimbres-Castro et al. (2013) to identify radiolarians.

Also there are a variety of methods in automatic classification and retrieval of plankton images. Segmenting the region of interest (ROI), feature extraction and finding a similarity or classifying image are the main steps of these systems. There are many image segmentation algorithms available e.g. thresholding-based, color-based, texture-based, model-based, etc. (Shapiro and Stockman, 2001). Wavelet descriptors (Arai, 2013; Landre and Truchetet, 2001) and morphological features like textural features (Hu and Davis, 2005), granulometric features (Luo et al., 2004; Zhao et al., 2010), the contour and boundary shape features (Arai and Rahmad, 2013; Rahmad and Arai, 2015), histogram of oriented gradients (HOG) (Bi et al., 2015), etc. are used commonly in the classification and image retrieval approaches. Fourier transform and Fourier masks are used in diatom and phytoplanktons image classification (Barajas-Garcia et al., 2016; Solorza and Alvarez-Borrego, 2015; Ventura et al., 2015).

Content-based image retrieval studies mainly focus on unsupervised matching unknown image to the known/labeled set of images and determining the similarity. Arai (2013), Arai and Rahmad (2013), Rahmad and Arai (2015) have used Euclidean distance, Landre and Truchetet (2001) have used iterative clustering as similarity measure. Compared to CBIR systems, classification approaches have studied more. SVM classifiers (Bi et al., 2015; Hu and Davis, 2005; Luo et al., 2004; Sosik and Olson, 2007); ensemble tree classifiers (Bell and Hopcroft, 2008; Zhao et al., 2010); discriminant classifiers (Li et al., 2014); statistical methods (Pearl et al., 2013); active learning approaches (Luo et al., 2005) are presented in several studies. There are semi-automatic classification studies, besides the automatic classification ones. Ye et al. (2011) proposed a Bayesian probabilistic model and Mike et al. (2016) proposed computational geometric model-based approach as semi-automatic methods. Deep learning is a new approach to machine learning that is being used in many research areas (Yu and Deng, 2011). The deep learning models must be trained with a large amount of data, and there are datasets with many instances available in plankton image studies (Sosik and Olson, 2007). Orenstein et al. (2015) proposed two convolutional neural network (CNN) approaches on plankton images. Al-Barazanchi et al. (2015) proposed hybrid CNN approaches for data collected with the shadowed imaged particle profiling and evaluation recorder (SIPPER) (Samson et al., 2002). Lee et al. (2016) presented a transfer learning approach and compared the results with CNN with/-without transfer learning.

The genera and species of the radiolarians are hard to determine because there are hundreds of species that vary in morphological features. Utilization of machine learning methods could ease this process as in the plankton image studies. The aim of this study is to help radiolarian paleontologists to be quicker in systematic studies and to help paleontologists to learn about the radiolarian systematics in a comprehensible way. In the proposed method, hand-crafted features (morphological and textural) and deep features are extracted and, feature selection is applied to select more discriminative features. Extracted features are grouped as hand-crafted, deep and combined sets. Classification algorithms are trained with these feature sets and results are analyzed.

In later sections, we first give details on experiment dataset, feature extraction and feature selection methods. In the experiment section, we present the classification methods and results. Finally, we discuss the results of our work and future plans.

2. Method

The flow of the proposed system can be divided into three main parts. First part is preprocessing step that consists segmentation of radiolarians. Pre-processing is made to select radiolarian body and remove unwanted structures. The second part is feature extraction. Hand-crafted and deep features are extracted from the extracted radiolarian silhouette. A pre-trained CNN is used to extract deep features. We use AlexNet (Krizhevsky et al., 2012) which is trained on Imagenet dataset. The activation values from the fully connected layers (Fc6, Fc7, and Fc8) of Alexnet are used as deep features. Each fully connected layer describes the image with a different abstraction. Deep features are high dimensional data, hence Relieff (Kononenko et al., 1997) feature selection algorithm is applied to select the strong features. The last step is the classification step and various classifiers are trained with selected deep and hand-crafted features for prediction. The trained models are tested with k-fold cross validation. In Fig. 1 the workflow of the proposed method is shown.

2.1. Dataset

There are 381 known Triassic radiolarian genera and most have been published since the 1970's following the introduction of Scanning Electron Microscopy (SEM). Seventy-three genera as synonyms and 11 genera as homonym were declared and 282 genera validated as Triassic in the organized image catalog of Mesozoic Radiolarians (O'Dogherty et al., 2009b), the revision made by the InterRad Mesozoic Working Group. In this study, the sample image data set is composed of SEM photographs of 27 species of Triassic radiolarians. Selected species have at least 10 sample images with good preservation and have high-quality SEM images through literature up until today and are chosen randomly from the studies carried around the world such as USA, Austria, Switzerland, Italy, Slovenia, Croatia, Slovenia, Serbia, Greece, Cyprus, Turkey, Japan, China, Thailand, Philippines and New Zealand which are cited in Table 1. In the literature, there are some hand-drawn radiolarian images from outdated literature or SEM images with bad preservation, some images of broken species or aff. and cf. of the species (samples without integrity). Most of the species does not have enough SEM images or images with good preservation. They are not taken into consideration. Sample radiolarian images of 4 different species are shown in Fig. 2.

The species in the dataset belong to three orders of radiolarians which are Entactinaria Kozur and Mostler (1982); Spumellaria Ehrenberg (1875) and Nassellaria Ehrenberg (1875). Mentioned species in the sample image data set are represented in Table 1.

2.2. Pre-processing

Due to varying image quality, a pre-processing step is applied to standardizing the images. Before feature extraction, non-image structures like tag characters or other text structures printed by the SEM imaging system should first be removed. In order to achieve this, a segmentation step is applied on images in the dataset. First, Otsu's thresholding method (Otsu, 1975) is applied on images, and binary maps are generated. Then, connected component analysis is applied to the binary image and the largest connected component is selected as radiolarian. Next, in the original image pixels that are not in the segmented binary mask is set to zero (0). In Fig. 3, original image, binary mask and segmented image are shown.

2.3. Features

After obtaining the mask, feature extraction is performed on the segmented image. Morphological, texture-based and deep features are extracted from each sample. The morphological features are eccentricity, solidity circularity, aspect ratio, area bounding box, moments and granulometric features. The texture features are Gabor features and wavelet moments. Some of these features like granulometric and GLCM are generally used in studies about microbiological studies (Arai, 2013; Arai and Rahmad, 2013; Bi et al., 2015; Rahmad and Arai, 2015). We utilize these features in our study too. The other morphological features and moment invariants are utilized however pure amorphous silica skeleton is the most distinct morphological feature of the radiolarians (De

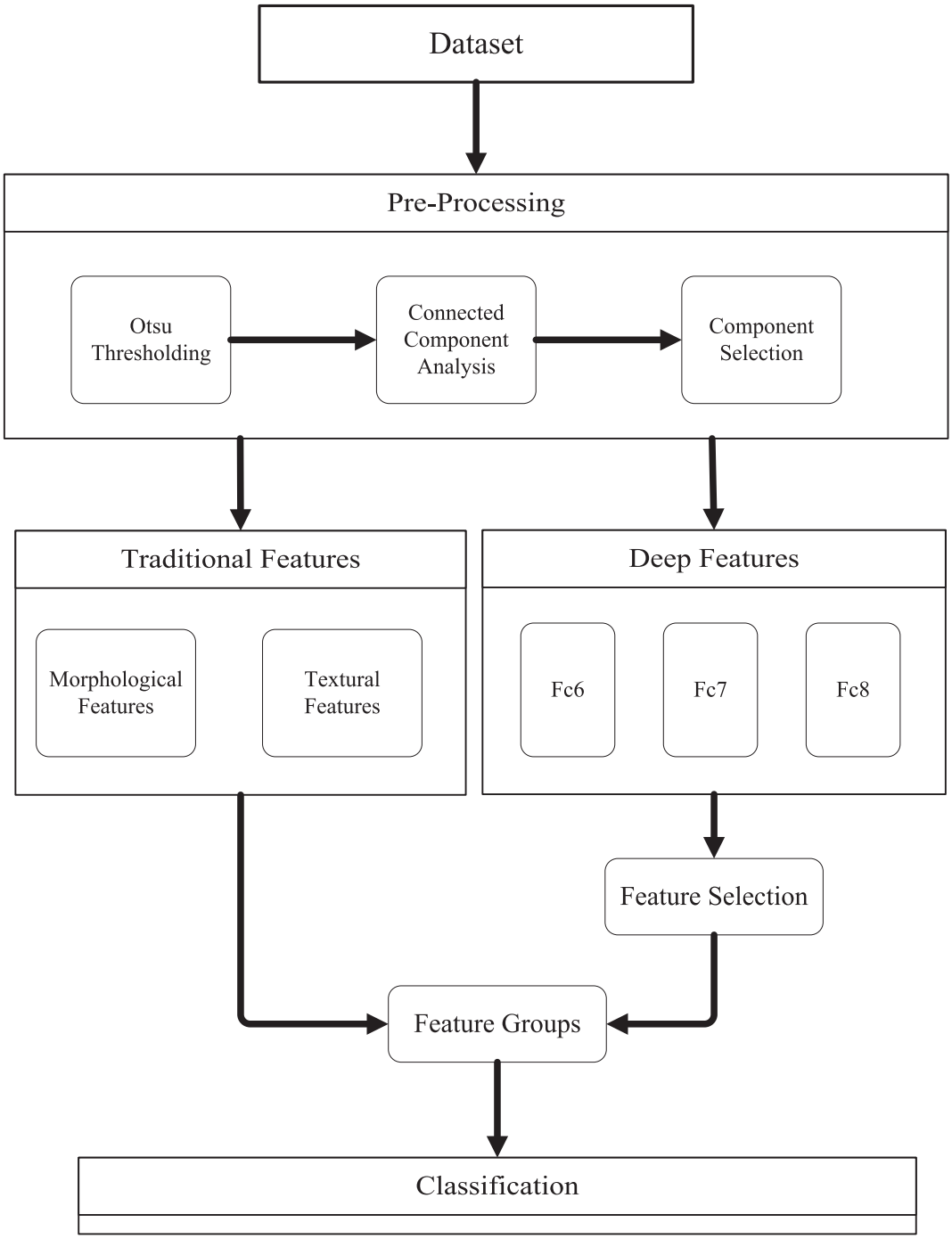

Fig. 1. The workflow for the proposed system.

Wever et al., 2002). These features are extracted from all images in the dataset. All of these features are explained below:

Eccentricity: The ratio of the distance between the foci of the ellipse and its major axis length. The eccentricity can also be interpreted as the fraction of the distance along the semi-major axis at which the focus lies.

Solidity: The ratio between the area of the object and the area of the convex hull.

Circularity: The measure of how close an object's shape is to a circle. Circularity is calculated by dividing perimeter to 4 π product area.

Aspect ratio: The ratio between the width and height of the object.

Area bounding box: The area of the bounding box that covers the object mask.

Granulometric features: These are computed by performing a series of morphological openings and closings (Luo et al., 2004). In each operation, different sized structure elements are used. The differences between subsequent operations are recorded in order to obtain these kinds of features. Granulometric features are robust to noise and contain inherent information of shape. Square-shaped structure elements are used. Granulometric features are computed as in Equation (1).

$$g_i = \frac{\#\ pixels\ changed\ after\ i^{th}\ operation}{\#\ pixels\ in\ original\ image} \tag{1}$$

Moment Invariants: These are features invariant to scaling, rotating and translating (Hu, 1962). If the image is a function of $f(x,y)$ then the $(p+q)th$ order moment is defined as in Equation (2).

Table 1
The literature used in the sample data set.

Species in the sample data set	The literature used in the sample data set
Betraccium deweveri Pessagno Jr and Blome, 1980	(Blome, 1984; Bragin, 1990; Carter and Orchard, 2007; Giordano et al., 2010; Pessagno Jr and Blome, 1980; Tekin, 2002)
Capnodoce anapates De Wever et al., 1979	(Bragin, 2007; De Wever et al., 1979; Nakaseko and Nishimura, 1979; Sugiyama, 1997; Uzuncimen et al., 2011)
Acanthotetrapaurinella variabilis Kozur and Mostler, 2006	(Dumitrica et al., 2013; Kozur and Mostler, 2006)
Triassospongosphaera multispinosa (Kozur and Mostler, 1979a)	(Bragin, 2011; Feng et al., 2009; Kozur and Mostler, 1979a; Ozsvárt and Kovács, 2012; Stockar et al., 2012; Tekin and Sonmez, 2010)
Capnuchosphaera colemani Blome, 1983	(Blome, 1983; Carter and Orchard, 2013; Tekin, 1999)
Pararchaeospongoprunum hermi Lahm, 1984	(Celarc et al., 2013; Kellici and De Wever, 1995; Kozur and Mostler, 1994; Lahm, 1984)
Vinassospongus subsphaericus Kozur and Mostler, 1979b	(Feng et al., 2005; Feng et al., 2009; Kozur and Mostler, 1979b; Lahm, 1984; Tekin, 1999; Tekin and Göncüoglu, 2007)
Eptingium manfredi Dumitrica, 1978	(Dumitrica, 1978; Kozur and Mostler, 1996; Ramovs and Gorican, 1995; Stockar et al., 2012)
Spongostephanidium longispinosum Sashida, 1991	(Kozur and Mostler, 1996; Marquez et al., 2006; Sashida, 1991; Sashida et al., 2000)
Hindeosphaera spinulosum (Nakaseko and Nishimura, 1979)	(Cheng, 1989; Feng et al., 2009; Goričan et al., 2005; Nakaseko and Nishimura, 1979; Yeh, 1990)
Pseudostylosphaera coccostyla coccostyla (Rüst, 1892)	(Feng et al., 2001; Kozur and Mostler, 1994; Sashida et al., 1999; Tekin, 1999)
Parasepsagon tetracanthus Dumitrica et al., 1980	(Dumitrica et al., 1980; Kellici and De Wever, 1995; Kozur and Mostler, 1982; Kozur and Mostler, 1994; Stockar et al., 2012)
Muelleritortis cochleata cochleata (Nakaseko and Nishimura, 1979)	(Kozur and Mostler, 1996; Nakaseko and Nishimura, 1979; Sugiyama, 1997; Tekin, 1999; Tekin and Göncüoglu, 2007)
Hungarosaturnalis latipannosus Mostler and Krainer, 1994	(Mostler and Krainer, 1994)
Tiborella florida florida (Nakaseko and Nishimura, 1979)	(Celarc et al., 2013; Feng et al., 2009; Kozur and Mostler, 1996; Nakaseko and Nishimura, 1979)
Pentactinocapsa awaensis (Nakaseko and Nishimura, 1979)	(Kozur and Mostler, 1994; Kozur and Mostler, 1996; Nakaseko and Nishimura, 1979; Ramovs and Gorican, 1995)
Canoptum rhaeticum Kozur and Mostler, 1981	(Kozur and Mostler, 1982; Sugiyama, 1997; Tekin, 1999, 2002; Uzuncimen et al., 2011)
Canesium lentum Blome, 1984	(Blome, 1984; Carter and Orchard, 2000; Tekin, 1999; Yoshida, 1986)
Corum regium Blome, 1984	(Aita and Sporli, 1994; Blome, 1984; Carter and Orchard, 2013; Yoshida, 1986)
Pachus multinodosus Tekin, 1999	(Carter and Orchard, 2013; Tekin, 1999)
Japonocampe nocva (Yao, 1982)	(Sugiyama, 1997; Tekin, 1999; Uzuncimen et al., 2011; Yao, 1982)
Livarella valida Yoshida, 1986	(Carter et al., 1993; Kojima and Mizutani, 1987; Yoshida, 1986)
Hozmadia reticulata Dumitrica et al., 1980	(Bragin, 1990; Celarc et al., 2013; Dumitrica et al., 1980; Kellici and De Wever, 1995; Ozsvárt and Kovács, 2012; Yeh, 1990)
Pseudosaturniforma carnica Kozur and Mostler, 1979a	(Kozur and Mostler, 1979a; Tekin, 1999; Tekin and Göncüoglu, 2007)
Triassocampe coronata Bragin, 1991	(Bragin, 1991; Celarc et al., 2013; Cordey, 1998; Sugiyama, 1992)
Yeharaia annulata Nakaseko and Nishimura, 1979	(Bragin, 1991; Celarc et al., 2013; Cordey, 1998; Kellici and De Wever, 1995; Kishida and Hisada, 1986; Kozur and Mostler, 1994; Nakaseko and Nishimura, 1979; Sugiyama, 1992; Yeh, 1990)
Xiphothecaella rugosa (Bragin, 1991)	(Bertinelli et al., 2005; Bortolotti et al., 2006; Bragin, 1991; Bragin, 2007; Tekin, 1999; Uzuncimen et al., 2011)

$$m_{pq} = \int_{-\infty}^{\infty}\int_{-\infty}^{\infty} x^p y^q f(x,y)dxdy \quad p,q = 1,2,3.... \tag{2}$$

The moments of seven orders are computed. m_{pq} is the moment sequence and is determined by the $f(x,y)$. Moments computed with Equation (2) may not be invariant to scaling, translating and rotating, so invariant features are obtained by calculating central moments. Central moments are calculated with Equation (3).

$$\mu_{pq} = \int_{-\infty}^{\infty}\int_{-\infty}^{\infty} (x-\bar{x})^p (y-\bar{y})^q f(x,y)dxdy \quad p,q = 1,2,3... \tag{3}$$

In Equation (3), $\bar{x}$ and $\bar{y}$ are the centroids of the image. The invariant moments are computed by shifting moment sequence to the center of the image. Through shifting, rotate and translate invariance are gained, and normalization is made for scale invariance. Normalized moments are defined with Equation (4).

$$n_{pq} = \frac{\mu_{pq}}{\mu^{\gamma}_{00}} \quad \gamma = \frac{p+q+2}{2}, \quad p+q = 2,3..... \tag{4}$$

Standard Deviation: The standard deviation of the pixels covered by the object mask.

Entropy: A metric that defines the complexity of the image. For example, a plain image's entropy is equal to zero. Entropy increases in direct proportion to an increase in image complexity (Gonzalez and Woods, 2007).

GLCM features: Twenty gray level co-occurrence matrix and Haralick texture features (Haralick and Shapiro, 1991) are extracted from the gray level image. Haralick features are contrast, correlation, energy, the sum of squares, the sum of average, the sum of variance, the sum of entropy, difference variance, difference entropy, and information measure of correlation. Other gray level co-occurrence matrix based features are autocorrelation, contrast, correlation, cluster prominence, cluster shade, dissimilarity, energy, entropy, homogeneity, maximum probability (Soh and Tsatsoulis, 1999) inverse difference normalized, and inverse difference moment normalized.

Gabor Features: Filters used for edge detection, but are also powerful tools in texture representation (Kamarainen, 2012).

The mean squared energy and mean amplitude for different scales and energy are computed. Filters in the filter bank are convolved with the image using FFT. After convolution, mean squared energy and mean amplitudes are then computed. Energy is computed by summing the response of the square of the filters and amplitude is computed by computing the mean of the filter responses.

Wavelet moments: Twenty features from the first two moments of wavelet coefficients (Papakostas et al., 2012) extracted from radiolarian images are selected. Initially, a 2-dimensional discrete wavelet transform is applied to the original gray image, then this process is repeated on the output of the previous processes for four times. Finally, mean and standard deviation of the final output (coefficients) is used as wavelet moment feature vector.

Deep Features: We use a pre-trained CNN (AlexNet) for deep feature extraction. CNNs are similar to common neural networks that comprised of neurons with weights and biases. Every neuron in a neural network receives some inputs and processes these inputs via an activation function. There are several kinds of layers in a CNN. These are input layer, convolution layers, pooling layers, rectified linear unit layers (RELU) and fully connected layers. Convolution layers are the main layers of the network. Convolution layer parameters are the learnable filters. Each filter is spatially small and extends through the input image. Each filter is convolved across the input and dot products between the input and the filter are computed. An activation map that gives the responses of corresponding filter at every spatial position is produced. Pooling layers take part between sequential convolution layers. Their function is to reduce the spatial size of the representation. The reduction of a number of parameters will reduce the computational cost. RELU layers apply an element-wise activation function and the size of the volume is unchanged after this operation. Fully connected layers compute the class scores. Neurons in a fully connected layer have full connections to all activations in the previous layer. A matrix multiplication followed by a bias offset is applied to compute their activations. AlexNet is a CNN model that is trained with ImageNet database. ImageNet contains millions of images from 22 K categories. All images are collected from the World Wide Web.

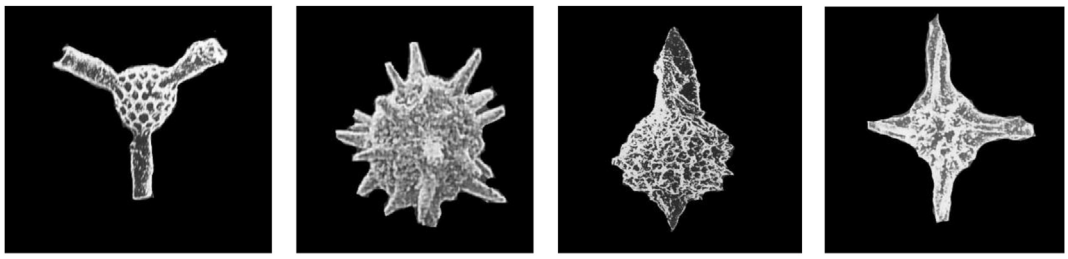

Fig. 2. Sample images of 4 radiolarian species.

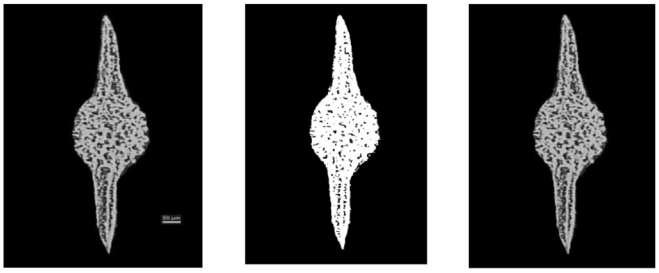

Fig. 3. (a) Original image, (b) Binary Mask, (c) Segmented image of a sample radiolarian.

Transfer learning is considered as the transfer of knowledge from one learned problem to a new task in machine learning (Pan and Yang, 2010). In the context of deep neural networks, it is transferring learned features of a pre-trained network to a new problem. We provide our radiolarian image set to AlexNet as input and obtain deep features from fully connected layers of this pre-trained CNN (fully connected layer 6 (Fc6), fully connected layer 7 (Fc7) and fully connected layer 8 (Fc8)). Representations learned at different layers of the deep neural networks correspond to different levels of abstraction of the input images. The input layer of the AlexNet is fixed, so all the input data is resized to 227 × 227 pixels and all grayscale images are converted to three channel by replication. Finally, we feed the CNN with the input images. Fc6, Fc7, and Fc8 features are concatenated and 10192 features are gathered. The CNN model is implemented in Caffe (Jia et al., 2014) which is a scientific computing framework.

Feature selection is applied over deep features to build a stronger feature set. In the feature selection process, a discriminative subset of features is selected by computing the weights of features. The weight is the strength of a feature. Selection is made by finding the subset that minimizes Bayesian error rate. The Relieff algorithm is selected cause of producing successful results with balanced datasets (Refaeilzadeh et al., 2007). Relieff method solves the multi-class and incomplete noisy data problems. A brief algorithm of Relieff is given in the appendix.

3. Experiments

Various predictive models are constructed with extracted features and different machine learning methods. Ten-fold cross-validation is used for model evaluation. In cross-validation, the dataset is split into *k* smaller sets. A model is trained using *k-1* folds of the training data. The resulting model is validated on the remaining fold. The performance measure reported is the average of the values computed in each iteration. k-fold cross validation reduced the overfitting by using independent test samples (Arlot and Celisse, 2010) and cross-validation is one solution to the lack of sufficiently large training and testing sets (Hart et al., 2001). Four kinds of classification methods are used in the experiments: function based Support Vector Machine (SVM) classifier, instance based k-Nearest Neighbor (kNN) classifier, ensemble based Adaboost classifier and ensemble tree based Random Forest (RF) classifier.

The linear kernel function is selected for SVM classifiers. The iteration count is not restricted and numerical tolerance is given as 0.001 to optimize the classifier. Fifty tree based estimators defined and learning rate is given as 0.1 in Adaboost classifier. Random Forest classifiers are trained with 100 trees and tree depth is not limited. In kNN algorithm, k value is set to 10 and instances are weighted according to Euclidean distances of features. Optimal k value is found by trials within 5–15.

The performance of classifiers is evaluated according to classification accuracy, sensitivity, specificity and area under curve metrics. In Table 2, the experiments with traditional size and texture features and transfer learning based deep features (Deep *N*) are compared. *N* is the percent of features reduced by using Relieff algorithm. While "Deep 10" denotes the best 10% of features selected according to their correspondence given by feature selection algorithm, "Deep 100" denotes no feature selection.

In Table 3, experiments with the combinations of hand-crafted features and deep features are given. Same classification metrics are provided as in Table 2. In the first column, "Combined *N*" denotes the percent of the reduction in deep features mentioned in Table 2.

According to the results of single group experiments in Table 2, SVM and RF classifiers provides the best results on all classification metrics with hand-crafted features. kNN classifier performs poorly on hand-crafted features with 28.2% classification accuracy but successfully on deep feature groups with 93.5% mean accuracy. The same difference also occurs on other classification metrics. RF and SVM classifiers on hand-

Table 2
Classification accuracy (*CA*), sensitivity (*Sens*), specificity (*Spec*) and area under curve (*AUC*) metrics for feature groups (hand-crafted features (*H-C*) and deep features (*Deep*)).

Feature Group	Classifier	CA	Sens	Spec	AUC
H-C	Adaboost	0.7340	0.6770	0.9861	0.8590
	kNN	0.2821	0.1457	0.9608	0.6020
	RF	0.8397	0.7906	0.9915	0.9180
	SVM	0.8494	0.7887	0.9921	0.9210
Deep 10	Adaboost	0.6474	0.5570	0.9813	0.8330
	kNN	0.9423	0.9150	0.9969	0.9670
	RF	0.9423	0.9222	0.9969	0.9800
	SVM	0.9840	0.9794	0.9992	0.9910
Deep 25	Adaboost	0.7019	0.6389	0.9842	0.8440
	kNN	0.9423	0.9150	0.9969	0.9670
	RF	0.9487	0.9334	0.9972	0.9720
	SVM	0.9808	0.9733	0.9990	0.9900
Deep 50	Adaboost	0.6763	0.6335	0.9827	0.8360
	kNN	0.9391	0.9100	0.9967	0.9660
	RF	0.9487	0.9330	0.9972	0.9780
	SVM	0.9840	0.9783	0.9991	0.9910
Deep 100	Adaboost	0.6635	0.6050	0.9820	0.8250
	kNN	0.9231	0.8894	0.9959	0.9570
	RF	0.9423	0.9289	0.9968	0.9670
	SVM	0.9840	0.9783	0.9991	0.9910

Table 3
Classification accuracy (CA), sensitivity (Sens), specificity (Spec) and area under curve (AUC) metrics for combined feature groups.

Feature Group	Classifier	CA	Sens	Spec	AUC
Combined 10	Adaboost	0.7212	0.6639	0.9853	0.8560
	kNN	0.8397	0.7897	0.9914	0.9130
	RF	0.9583	0.9451	0.9978	0.9770
	SVM	0.9872	0.9808	0.9993	0.9930
Combined 25	Adaboost	0.7308	0.6632	0.9858	0.8500
	kNN	0.8910	0.8584	0.9941	0.9390
	RF	0.9519	0.9355	0.9974	0.9770
	SVM	0.9840	0.9775	0.9992	0.9920
Combined 50	Adaboost	0.6955	0.6345	0.9840	0.8400
	kNN	0.8910	0.8544	0.9941	0.9390
	RF	0.9583	0.9459	0.9977	0.9710
	SVM	0.9840	0.9783	0.9991	0.9910
Combined 100	Adaboost	0.6859	0.6256	0.9834	0.8330
	kNN	0.9103	0.8785	0.9951	0.9490
	RF	0.9423	0.9297	0.9968	0.9670
	SVM	0.9840	0.9783	0.9991	0.9910

Table 4
McNemar's test p-value's of deep feature groups vs. traditional feature group for RF and SVM classifiers.

Feature Groups	Hand-Crafted (SVM)	Hand-Crafted (RF)
Deep 10	<0.001	<0.001
Deep 25	<0.001	<0.001
Deep 50	<0.001	<0.001
Deep 100	<0.001	<0.001

crafted features provide similar and successful results with 84% and 85% classification accuracy respectively. They have similar sensitivity (79%, 78.9%), specificity (99.2%, 98.1%) and area under curve (91.8%, 92.1%) outputs.

According to combined group experiment results in Table 3, Adaboost classifier's performance improved for deep features, but still lower than the single hand-crafted feature set classification. RF algorithm has the most improvement on classification accuracy and sensitivity with combined features by 1% and 2% respectively. kNN classifier's performance has reduced by around 10% and SVM classifier provides similar results as in single group results.

When comparing the general classifier outputs, hand-crafted feature and 10% of deep feature combination provide the best classification performance on SVM classifier (CA: 98.7%, Sens: 98.1%, Spec: 99.9%, AUC: 99.3%). Deep features are practically more successful on defining radiolarian images than hand-crafted features. To analyze this situation deeply, statistical significance tests are applied on deep feature groups versus traditional feature group and combined feature groups versus deep feature groups.

McNemar's test (McNemar, 1947) is used to compare the statistical significance between classification outcomes of the two methods. This test measures if a statistically significant change in proportions have occurred on a dichotomous (true/false or successful/unsuccessful) data, can be used to compare two classification approach. In Table 4, deep features and hand-crafted features are compared with two most successful classifiers, RF and SVM. According to results, all deep groups vs. hand-crafted features have significant classification outcomes ($p < 0.001$). In Table 5, deep features and combined features are compared with, RF and SVM classifiers as in Table 4. This once, there is no statistical difference in the proportion of samples classified by all methods ($p > 0.05$). With these test results and the results from Table 2, we can conclude that using deep features are more successful on the classification of radiolarians and; combining the hand-crafted and the deep features are unnecessary.

Although the performance of the classifiers on all *Deep* and *Combined* feature groups are close, reducing the feature size facilitates the time complexity and interpretability of classification methods. 10% percent of the feature size reduces the mean execution time of the classifiers by %36 comparing to 100% feature size.

4. Conclusion

For radiolarian paleontologists, extracting techniques and taxonomic studies are time-consuming processes, despite it is one of the low cost and a trustworthy way to obtain dating of deep ocean sediments beside geochemistry (O'Dogherty et al., 2009a). An expert should review the whole catalog and compare with the previous samples to find out the genus and specie of the radiolarian. The literature consist of hundreds of images and review of this literature can sometimes take days according to paleontologists' experience. Predicting the species of unknown samples automatically will help the experts to gain time in taxonomic studies.

In this paper, a method that uses hand-crafted and deep features to automatically classify radiolarian species is proposed. Although there are many studies exists on plankton classification, there are limited number of studies on classification of radiolarians. In this study, we applied transfer learning methods on Radiolarian images, compared the hand-crafted and deep features, and analyzed the different classification methods. Another contribution of the study is collecting a dataset from radiolarian research literature for evaluation. The selected species have high-quality SEM images and have at least 10 sample images through literature. Dataset can be expanded with the new SEM images provided by researchers.

Our method consists of three steps: segmentation of radiolarian, feature extraction and weighting, and classification. First, Otsu's method used for segmentation and the unrelated parts of the radiolarian images are removed. After, hand-crafted features, deep features from a pre-trained CNN and the combination of both are extracted. Relieff algorithm is used for feature selection on deep features to obtain strong and robust image descriptors. Finally, four different well-known machine learning methods are used for classification. The experimental results are analyzed according to classification performance and statistical significance. The results show that deep features provides superior classification outcomes against hand-crafted features. We also observed that combining hand-crafted and deep features has not a meaningful effect on classification accuracy.

Even though the proposed method has focused on Radiolarian images, similar mechanisms can be developed for classification and recognition of fossil images such as foraminiferas, ostracodas and etc. The limitation of the proposed method is the lack of semantic information of radiolarians e.g. age, period, location. For future work, we plan to expand the feature set by using additional features such as scale-invariant features and provide the semantic information. By these improvements, biostratigraphic studies and paleogeographic interpretations could be made more easily. The method described here is a step toward the long-term goal of highly-accurate automatic classification of radiolarians.

Table 5
McNemar's test p-value's of combined features groups vs. deep feature groups for RF and SVM classifiers.

Feature Groups	Deep 10 (SVM)	Deep 25 (SVM)	Deep 50 (SVM)	Deep 100 (SVM)	Deep 10 (RF)	Deep 25 (RF)	Deep 50 (RF)	Deep 100 (RF)
Combined 10	0.3170	0.3173	0.6547	0.6547	0.1317	0.4386	0.4054	0.1655
Combined 25	1.000	0.3173	1.000	1.000	0.3657	0.7630	0.7389	0.4386
Combined 50	1.000	0.3173	0.998	1.000	0.1317	0.3137	0.4054	0.1655
Combined 100	1.000	0.5637	1.000	1.000	1.000	0.6171	0.5930	1.000

APPENDIX

Relieff Algorithm

A brief algorithm of Relieff is given below:

w[1..*n*] = 0 *(Set all weights to 0)*
For i=1:m do
  Randomly select an instance r_i
  Find k nearest hits h_i
  For each class C≠class(r_i) *do*
    Find misses $m_j(c)$ *from class C*
    For A:=1 to n (number of attributes) do

$$w[A] = w[A] - \sum_{j=1}^{k} \frac{diff(A, r_i, h_i)}{(m,k)} + \sum_{C \neq class(r_i)} \frac{\left[\frac{p(c)}{1-p(class(r_i))} \sum_{j=1}^{k} \frac{diff(A, r_i, h_i)}{(m,k)}\right]}{(m,k)}$$

In the algorithm, m denotes the number of instances, A denotes an attribute, n denotes the number of attributes, $w[A]$ denotes the weight of A, p denotes the probability of an event. *diff()* function calculates differences. The output of the algorithm w is the weight of the features.

References

Aita, Y., Sporli, K., 1994. Late Triassic radiolaria from the Torlesse Terrane, Rimutaka range, North Island, New Zealand. N. Z. J. Geol. Geophys. 37, 155–162.

Al-Barazanchi, H.A., Verma, A., Wang, S., 2015. Performance evaluation of hybrid CNN for SIPPER plankton image classification. In: 2015 Third International Conference on Image Information Processing (Iciip), pp. 551–556.

Apostol, L.A., Márquez, E., Gasmen, P., Solano, G., 2016. RadSS: a radiolarian classifier using support vector machines. In: 2016 7th International Conference on Information, Intelligence, Systems & Applications (IISA), pp. 1–6.

Arai, K., 2013. Image Retrieval and Classification Method Based on Euclidian Distance between Normalized Features Including Wavelet Descriptor. Image 2.

Arai, K., Rahmad, C., 2013. Content based image retrieval by using multi layer centroid contour distance. Int. J. Adv. Res. Artif. Intell. 2.

Arlot, S., Celisse, A., 2010. A survey of cross-validation procedures for model selection. Stat. Surv. 4, 40–79.

Barajas-Garcia, C., Solorza-Calderon, S., Alvarez-Borrego, J., 2016. Classification of fragments of objects by the Fourier masks pattern recognition system. Opt. Commun. 367, 335–345.

Bell, J.L., Hopcroft, R.R., 2008. Assessment of ZooImage as a tool for the classification of zooplankton. J. Plankton Res. 30, 1351–1367.

Bertinelli, A., Ciarapica, G., Passeri, L., 2005. Late Triassic-Jurassic basinal successions in Molise and northern Basilicata; the northernmost witness of the Ionian Ocean. Boll. della Soc. Geol. Ital. 124, 177–188.

Bi, H., Guo, Z., Benfield, M.C., Fan, C., Ford, M., Shahrestani, S., Sieracki, J.M., 2015. A semi-automated image analysis procedure for in situ plankton imaging systems. PloS One 10 e0127121.

Blome, C.D., 1983. Upper Triassic capnuchosphaeridae and capnodocinae (radiolaria) from east-central oregon. Micropaleontology 11–49.

Blome, C.D., 1984. Upper Triassic Radiolaria and Radiolarian Zonation from Western North America.

Bortolotti, V., Chiari, M., Kodra, A., Marcucci, M., Marroni, M., Mustafa, F., Prela, M., Pandolfi, L., Principi, G., Saccani, E., 2006. Triassic MORB magmatism in the southern Mirdita zone (Albania). Ofioliti 31, 1–9.

Bragin, N.Y., 1990. Triassic Biostratigraphy of Radiolarian Deposits in Eastern USSR. Radiolarian Biostratigraphy, Academy of Science of the USSR (Urals Department), pp. 26–31.

Bragin, N.Y., 1991. Pozdnetriasovie radiolarii saturnalidae deflandre pravoberejiar amura. In: Tochilino, S.V. (Ed.), Palaeont. Stra. Inves. of Phanareozoic in the Far Eastern Region, pp. 100–103.

Bragin, N.Y., 2007. Late Triassic radiolarians of Southern Cyprus. Paleontol. J. 41, 951–1029.

Bragin, N.Y., 2011. Triassic radiolarians of Kotel'nyi Island (New Siberian Islands, Arctic). Paleontol. J. 45, 711–778.

Carter, E.S., Guex, J., Joseph, C., Baumgartner, P., Baud, A., Dumitrica, P., Hirsch, F., 1993. Biochronology and Paleontology of Uppermost Triassic (Rhaetian) Radiolarians, Queen Charlotte Islands, British Columbia, Canada.

Carter, E.S., Orchard, M., 2000. Intercalibrated Conodont-radiolarian Biostratigraphy and Potential Datums for the Carnian-norian Boundary within the Upper Triassic Peril Formation, Queen Charlotte Islands, British Columbia. Natural Resources Canada, Geological Survey of Canada.

Carter, E.S., Orchard, M.J., 2007. Radiolarian-conodont-ammonoid intercalibration around the Norian-Rhaetian boundary and implications for trans-Panthalassan correlation. Albertiana 36, 149–163.

Carter, E.S., Orchard, M.J., 2013. Intercalibration of Conodont and Radiolarian Faunas from the Carnian-Norian Boundary Intervalin Haidagwaii, British Columbia, Canada, vol. 61. The Triassic System: New Developments in Stratigraphy and Paleontology: Bulletin, pp. 61–67.

Casey, R.E., Weinheimer, A.L., Nelson, C.O., 1990. Cenozoic radiolarian evolution and zoogeography of the Pacific. Bull. Mar. Sci. 47, 221–232.

Celarc, B., Goričan, Š., Kolar-Jurkovšek, T., 2013. Middle Triassic carbonate-platform break-up and formation of small-scale half-grabens (Julian and Kamnik–Savinja Alps, Slovenia). Facies 59, 583–610.

Cheng, Y., 1989. Upper Paleozoic and Lower Mesozoic Radiolarian Assemblages from the Busuanga Islands, North Palawan Block, Philippines, vol. 1. Bulletin of the National Museum of Natural Science, Taiwan, pp. 129–175.

Cordey, F., 1998. Radiolaires des complexes d'accrétion de la Cordillère Canadienne (Colombie-Britannique). Commission géologique du Canada.

De Wever, P., Dumitrica, P., Caulet, J.P., Nigrini, C., Caridroit, M., 2002. Radiolarians in the Sedimentary Record. CRC Press.

De Wever, P., Sanfilippo, A., Riedel, W., Gruber, B., 1979. Triassic radiolarians from Greece, Sicily and Turkey. Micropaleontology 75–110.

Dumitrica, P., 1978. Family Eptingiidae n. fam., Extinct Nassellaria (Radiolaria) with Sagittal Ring, vol. 64. Dari de seama ale sedintelor, Institutul de Geologie si Geofizica, Bucharest, pp. 27–38.

Dumitrica, P., Kozur, H., Mostler, H., 1980. Contribution to the radiolarian fauna of the Middle Triassic of the Southern Alps. Geol. Paläontol. Mittl. Innsbr. 10, 1–46.

Dumitrica, P., Tekin, U.K., Bedi, Y., 2013. Taxonomic study of the tetrahedral, pentagonal and hexagonal spongy spumellarian Radiolaria from the middle Carnian (Late Triassic) of the Koseyahya nappe (Elbistan, SE Turkey) and other Triassic localities. Palaeontol. Z. 87, 311–343.

Ehrenberg, C.G., 1875. Fortsetzung der mikrogeologischen Studien, als Gesammt-Uebersicht der mikroskopischen Paläontologie gleichartig analysirter Gebirgsarten der Erde: mit specieller Rücksicht auf den Polycystinen-Mergel von Barbados. Buchdr. der K. Akademie der Wissenschaften, in Commission bei F. Dümmler.

Feng, Q., Chonglakmani, C., Helmcke, D., Ingavat-Helmcke, R., Liu, B., 2005. Correlation of Triassic stratigraphy between the Simao and Lampang-Phrae Basins: implications for the tectonopaleogeography of Southeast Asia. J. Asian Earth Sci. 24, 777–785.

Feng, Q., Yang, Z., Li, X., Crasquin, S., 2009. Middle and Late Triassic radiolarians from northern Tibet: implications for the Bayan Har Basin evolution. Geobios 42, 581–601.

Feng, Q., Zhang, Z., Gu, S., Ye, M., 2001. Radiolarian fauna from the Permian-Triassic transition. Geol. Sci. Technol. Inf. 20, 31–34.

Fimbres-Castro, C., Alvarez-Borrego, J., Vazquez-Martinez, I., Espinoza-Carreon, T.L., Ulloa-Perez, A.E., Bueno-Ibarra, M.A., 2013. Nonlinear correlation by using invariant identity vectors signatures to identify plankton. Gayana 77, 105–124.

Giordano, N., Rigo, M., Ciarapica, G., Bertinelli, A., 2010. New biostratigraphical constraints for the Norian/Rhaetian boundary: data from Lagonegro Basin, Southern Apennines, Italy. Lethaia 43, 573–586.

Gonzalez, R.C., Woods, R.E., 2007. Image Processing. Digital image processing 2.

Goričan, Š., Halamić, J., Grgasović, T., Kolar-Jurkovšek, T., 2005. Stratigraphic evolution of Triassic arc-backarc system in northwestern Croatia. Bull. Soc. Géol. Fr. 176, 3–22.

Haralick, R.M., Shapiro, L.G., 1991. Computer and Robot Vision. Addison-Wesley Longman Publishing Co., Inc.

Hart, P.E., Stork, D.G., Duda, R.O., 2001. Pattern Classification. John Willey & Sons.

Hu, M.-K., 1962. Visual pattern recognition by moment invariants. IRE Trans. Inf. Theory 8, 179–187.

Hu, Q., Davis, C., 2005. Automatic plankton image recognition with co-occurrence matrices and support vector machine. Mar. Ecol. Prog. Ser. 295, 21–31.

Jia, Y., Shelhamer, E., Donahue, J., Karayev, S., Long, J., Girshick, R., Guadarrama, S., Darrell, T., 2014. Caffe: convolutional architecture for fast feature embedding. In: Proceedings of the 22nd ACM International Conference on Multimedia. ACM, pp. 675–678.

Kamarainen, J.-K., 2012. Gabor features in image analysis, Image Processing Theory, Tools and Applications (IPTA). In: 2012 3rd International Conference on. IEEE, pp. 13–14.
Kellici, I., De Wever, P., 1995. Radiolaries Triasiques du Massif de la Marmolada, Italie du Nord. Rev. Micropaléontol. 38, 139–167.
Kishida, Y., Hisada, K., 1986. Radiolarian assemblages of the Sambosan Belt in the western part of the Kanto Mountains, Central Japan. News Osaka Micropaleontol. Spec. Vol. 7, 25–34.
Kojima, S., Mizutani, S., 1987. Triassic and Jurassic Radiolaria from the Nadanhada Range, Northeast China. Nihon Koseibutsu Gakkai hokoku, kiji, pp. 256–275.
Kononenko, I., Simec, E., RobnikSikonja, M., 1997. Overcoming the myopia of inductive learning algorithms with RELIEFF. Appl. Intell. 7, 39–55.
Kozur, H., Mostler, H., 1979a. Beiträge zur Erforschung der mesozoischen Radiolarien. Teil IV. Thalassosphaeracea HAECKEL, 1862, Hexastylacea HAECKEL, 1862 emend Petrushevskaya 1979, Sponguracea HAECKEL, 1862 emend. und weitere triassische Lithocycliacea, Trematodiscacea, Actinommacea und Nassellaria. Geol. Paläontol. Mittl. Innsbr. 1, 1–208.
Kozur, H., Mostler, H., 1979b. Eine neue Radiolariengattung aus dem höheren Cordevol (Unterkarn) von Göstling (Österreich). Institut für Geologie und Paläontologie.
Kozur, H., Mostler, H., 1981. Teil IV: Thalassosphaeracea Haeckel, 1862, Hexastylacea Haeckel, 1882, emend. Petrushevskaja, 1979, Sponguracea Haeckel, 1862 emend. und weitere triassische Lithocycliacea, Trematodiscacea, Actinommacea und Nassellaria, vol. 1. Geologisch-Paläontologische Mitteilungen, Innsbruck, Sonderband, p. 208.
Kozur, H., Mostler, H., 1982. Entactinaria Subordo nov., a New Radiolarian Suborder. Institut für Geologie und Paläontologie.
Kozur, H., Mostler, H., 1994. Anisian to Middle Carnian radiolarian zonation and description of some stratigraphically important radiolarians. Geol. Paläontol. Mittl. Innsbr. 3, 39–255.
Kozur, H., Mostler, H., 1996. Longobardian (late Ladinian) Muelleritortiidae (Radiolaria) from the Republic of Bosnia-Hercegovina. Geol. Paläontol. Mittl. Innsbr. 4, 83–103.
Kozur, H., Mostler, H., 2006. Radiolarien aus dem Longobard der Dinariden. Hallesches Jahrb. für Geowiss. 28, 23–91.
Krizhevsky, A., Sutskever, I., Hinton, G.E., 2012. Imagenet classification with deep convolutional neural networks. In: Advances in Neural Information Processing Systems, pp. 1097–1105.
Lahm, B., 1984. Spumellarienfaunen (Radiolaria) aus den mitteltriassischen Buchensteiner-Schichten von Recoaro (Norditalien) und den obertriassischen Reiflingerkalken von Grossreifling (Österreich): Systematik, Stratigraphie. F. Pfeil.
Landre, J., Truchetet, F., 2001. Hierarchical architecture for content-based image retrieval of paleontology images, Electronic Imaging 2002. Int. Soc. Opt. Photonics 138–147.
Lee, H., Park, M., Kim, J., 2016. Plankton classification on imbalanced large Scale database via convolutional neural networks with transfer learning. In: 2016 IEEE International Conference on Image Processing (Icip), pp. 3713–3717.
Li, Z.F., Zhao, F., Liu, J.Z., Qiao, Y., 2014. Pairwise nonparametric discriminant analysis for binary plankton image recognition. IEEE J. Ocean. Eng. 39, 695–701.
Luo, T., Kramer, K., Goldgof, D.B., Hall, L.O., Samson, S., Remsen, A., Hopkins, T., 2004. Recognizing plankton images from the shadow image particle profiling evaluation recorder. IEEE Trans. Syst. Man Cybern. Part B (Cybernetics) 34, 1753–1762.
Luo, T., Kramer, K., Goldgof, D.B., Hall, L.O., Samson, S., Remsen, A., Hopkins, T., 2005. Active learning to recognize multiple types of plankton. J. Mach. Learn. Res. 6, 589–613.
Marquez, E.J., Aitchison, J.C., Zamoras, L.R., 2006. Upper Permian to Middle Jurassic radiolarian assemblages of Busuanga and surrounding islands, Palawan, Philippines. Eclogae Geol. Helvetiae 99, S101–S125.
McNemar, Q., 1947. Note on the sampling error of the difference between correlated proportions or percentages. Psychometrika 12, 153–157.
Mike, J., Sumrall, C.D., Maroulas, V., Schwartz, F., 2016. Nonlandmark classification in paleobiology: computational geometry as a tool for species discrimination. Paleobiology 42, 696–706.
Mostler, H., Krainer, K., 1994. Saturnalidae radiolarien aus dem Langobard der südalpinen Karawanken (Kärnten, Österreich). Geol. Paläontol. Mittl. Innsbr. 19, 93–131.
Nakaseko, K., Nishimura, A., 1979. Upper Triassic radiolaria from southwest Japan. Sci. Rep. Coll. Gen. Educ. Osaka Univ. 28, 61–109.
O'Dogherty, L., Carter, E.S., Dumitrica, P., Gorican, S., De Wever, P., 2009a. An illustrated and revised catalogue of Mesozoic radiolarian genera - objectives, concepts and guide for users. Geodiversitas 31, 191–212.
O'Dogherty, L., Carter, E.S., Dumitrica, P., Goriččan, Š., De Wever, P., Hungerbühler, A., Bandini, A.N., Takemura, A., 2009b. Catalogue of Mesozoic radiolarian genera. Part 1: Triassic. Geodiversitas 31, 213–270.
Orenstein, E.C., Beijbom, O., Peacock, E.E., Sosik, H.M., 2015. Whoi-Plankton-a Large Scale Fine Grained Visual Recognition Benchmark Dataset for Plankton Classification arXiv preprint arXiv:1510.00745.
Otsu, N., 1975. A threshold selection method from gray-level histograms. Automatica 11, 23–27.
Ozsvárt, P., Kovács, S., 2012. Revised Middle and Late Triassic radiolarian ages for ophiolite mélanges: implications for the geodynamic evolution of the northern part of the early Mesozoic Neotethyan subbasins. Bull. Soc. Géol. Fr. 183, 273–286.
Pan, S.J., Yang, Q., 2010. A survey on transfer learning. IEEE Trans. Knowl. Data Eng. 22, 1345–1359.
Papakostas, G., Koulouriotis, D., Tourassis, V., 2012. Feature Extraction Based on Wavelet Moments and Moment Invariants in Machine Vision Systems. INTECH Open Access Publisher.
Pearl, M.R., Swanstrom, J.A., Bruckman, L.S., Richardson, T.L., Shaw, T.J., Sosik, H.M., Myrick, M.L., 2013. Taxonomic classification of phytoplankton with Multivariate optical computing, Part III: demonstration. Appl. Spectrosc. 67, 640–647.
Pessagno Jr., E.A., Blome, C.D., 1980. Upper Triassic and Jurassic Pantanelliinae from California, Oregon and British Columbia. Micropaleontology 225–273.
Pessagno Jr., E.A., Newport, R.L., 1972. A technique for extracting Radiolaria from radiolarian cherts. Micropaleontology 231–234.
Rahmad, C., Arai, K., 2015. Comparison contour extraction based on layered Structure and fourier descriptor on image retrieval. Int. J. Adv. Comput. Sci. Appl. 6, 71–74.
Ramovs, A., Gorican, S., 1995. Late Anisian-early Ladinian Radiolarians and Conodonts from Smarna Gora Near Ljubljuna, Slovenia. Razprave 4, Razrsozu 36, pp. 179–221.
Refaeilzadeh, P., Tang, L., Liu, H., 2007. On comparison of feature selection algorithms. In: Proceedings of AAAI Workshop on Evaluation Methods for Machine Learning II, p. 5.
Rüst, D., 1892. Radiolaria from Pierre formation of North-western Manitoba, vol. 4. Geological and Natural History Survey of Canada. Contributions to the Canadian Micropalaeontology, pp. 101–110.
Samson, S., Langebrake, L., Patten, J., Lembke, C., 2002. Shadowed Image Particle Profiling and Evaluation Recorder. Google Patents.
Sashida, K., 1991. Early Triassic radiolarians from the Ogamato formation, Kanto Mountains, Central Japan, Part 2. Trans. Proc. Paleont. Soc. Jpn. N. Ser. 161, 681–696.
Sashida, K., Kamata, Y., Adachi, S., Munasri, 1999. Middle Triassic radiolarians from West Timor, Indonesia. J. Paleontol. 73, 765–786.
Sashida, K., Nakornsri, N., Ueno, K., Sardsud, A., 2000. Carboniferous and Triassic Radiolarian Faunas from the Saba Yoi Area, Southrenmost Part of Peninsular Thailand and Their Paleogeographic Significance. Science Reports of the Institute of Geoscience, University of Tsukuba, Section B, Geological Sciences, pp. 71–100.
Shapiro, L.G., Stockman, G.C., 2001. Computer Vision. Prentice-Hall, New Jersey.
Soh, L.K., Tsatsoulis, C., 1999. Texture analysis of SAR sea ice imagery using gray level co-occurrence matrices. IEEE Trans. Geosci. Remote Sens. 37, 780–795.
Solorza, S., Alvarez-Borrego, J., 2015. Position and rotation-invariant pattern recognition system by binary rings masks. J. Mod. Opt. 62, 851–864.
Sosik, H.M., Olson, R.J., 2007. Automated taxonomic classification of phytoplankton sampled with imaging-in-flow cytometry. Limnol. Oceanogr. 5, 204–216.
Stockar, R., Dumitrica, P., Baumgartner, P.O., 2012. Early Ladinian radiolarian fauna from the Monte san Giorgio (southern Alps, Switzerland): Systematics, biostratigraphy and paleo (bio) geographic implications. Riv. Italiana di Paleontol. e Stratigr. (Res. Paleontol. Stratigr.) 118.
Sugiyama, K., 1992. 941. Lower and Middle Triassic Radiolarians from Mt. Kinkazan, Gifu Prefecture, Central Japan, Transactions and Proceedings of the Paleontological Society of Japan. New series. Palaeontological Society of Japan, pp. 1180–1223.
Sugiyama, K., 1997. Triassic and Lower Jurassic Radiolarian biostratigraphy in the siliceous claystone and bedded chert units of the southeastern Mino Terrane, Central Japan. Bull. Mizunami Fossil Mus. 24, 79–193.
Tekin, U.K., 1999. Biostratigraphy and systematics of late Middle to late Triassic radiolarians from the Taurus Mountains and Ankara region, Turkey. Geol. Paläontol. Mittl. Innsbr. 5, 1–297.
Tekin, U.K., 2002. Late Triassic (Late Norian-Rhaetian) radiolarians from the Antalya Nappes, central Taurides, Southern Turkey. Riv. Ital. Di Paleontol. E Stratigr. 108, 415–440.
Tekin, U.K., Göncüoglu, M.C., 2007. Discovery of the oldest (Upper Ladinian to Middle Carnian) radiolarian assemblages from the Bornova flysch zone in western Turkey: implications for the evolution of the Neotethyan Izmir-Ankara ocean. Ofioliti 32, 131–150.
Tekin, U.K., Sonmez, I., 2010. Late Ladinian radiolarians from the Tahtalidag Nappe of the Antalya nappes, SW Turkey: remarks on the late Middle and Late Triassic evolution of the Tahtalidag Nappe. Acta Geol. Pol. 60, 199–217.
Uzuncimen, S., Tekin, U.K., Bedi, Y., Perincek, D., Varol, E., Soycan, H., 2011. Discovery of the Late Triassic (Middle Carnian-Rhaetian) radiolarians in the volcano-sedimentary sequences of the Kocali Complex, SE Turkey: correlation with the other Tauride units. J. Asian Earth Sci. 40, 180–200.
Ventura, A.S., Borrego, J.A., Solorza, S., 2015. Adaptive nonlinear correlation with a binary mask invariant to rotation and scale. Opt. Commun. 339, 185–193.
Yao, A., 1982. Middle Triassic to Early Jurassic Radiolarians from the Inuyama Area. central Japan.
Ye, L., Chang, C.Y., Hsieh, C.H., 2011. Bayesian model for semi-automated zooplankton classification with predictive confidence and rapid category aggregation. Mar. Ecol. Prog. Ser. 441, 185–196.
Yeh, K., 1990. Taxonomic studies of Triassic Radiolaria from Busuanga Island, Philippines, 2. Bulletin of the National Museum of Natural Science, Taiwan, pp. 1–63.
Yoshida, H., 1986. Upper Triassic to lower Jurassic radiolarian biostratigraphy in Kagamigahara city, Gifu Prefecture, Central Japan. J. Earth Sci. 34, 1–21.
Yu, D., Deng, L., 2011. Deep learning and its applications to signal and information processing [exploratory dsp]. IEEE Signal Process. Mag. 28, 145–154.
Zhao, F., Lin, F., Seah, H.S., 2010. Binary SIPPER plankton image classification using random subspace. Neurocomputing 73, 1853–1860.